SPACELAB
DIFFUSE SOFT X-RAY BRAGG SPECTROMETER
(DXS)

W. T. Sanders, Principal Investigator
R. J. Paulos, Program Manager

Space Science and Engineering Center
University of Wisconsin-Madison
1225 West Dayton Street
Madison, WI 53706

FINAL REPORT
NASA Contract NAS 5-26078

March 29, 1996

1 Summary

The Diffuse X-ray Spectrometer (DXS) is a Spacelab payload that was proposed and funded in response to NASA AO-OSS-2-78. The experiment was constructed under contract to NASA at the University of Wisconsin, with payload support, calibration and data analysis also provided by the University of Wisconsin. DXS was flown as an attached Shuttle payload on the STS-54 mission, which was launched from the Kennedy Space Center on Wednesday, 13 January 1993, and landed at Edwards Air Force Base on Tuesday, 19 January 1993.

DXS consists of a pair of Bragg crystal spectrometers that employ position-sensitive proportional counters as the x-ray detectors. DXS obtained the spectrum of the low energy x-ray diffuse background over the wavelength range 44 – 84 Å with spectral resolution 2 – 3 Å. The region of sky covered was an arc 15° wide approximately along the Galactic plane extending from longitude 150° to 300°.

For the past 25 years, the low energy x-ray diffuse background has been interpreted as thermal emission from a hot plasma in the interstellar medium, but there was no direct proof of its thermal nature. The primary scientific objective of the DXS experiment was to determine if the low energy x-ray diffuse background emission was thermal by determining if there were emission lines in its spectrum. Other important objectives were to determine if the plasma is in thermal equilibrium, to find the temperature of the plasma, to learn which chemical elements are the dominant emitters, and to determine the degree of depletion or enrichment of these elements in the emitting plasma relative to "standard" cosmic abundances.

The primary DXS activities following the DXS mission have been trouble-shooting an in-flight performance anomaly, vacuum-tank calibration of the instruments, preparation of an archival quality data set, and analysis of the calibration and flight data.

The major scientific result from the DXS analysis is the detection of lines in the spectrum of the low energy x-ray diffuse background, confirming the thermal nature of the emission. A second major result is the finding that the measured spectra do not look like the "standard" equilibrium temperature models, suggesting either that the models are not very accurate or that reality is not very simple, or both.

2 Description of DXS Payload

The Diffuse X-ray Spectrometer (DXS) is an attached Shuttle payload that flew on the January 1993 flight of STS-54. It consists of two identical Bragg crystal spectrometer instruments that are mounted one on either side of the Shuttle cargo bay. Figure 1 shows the layout of one DXS instrument. Each instrument, Port and Starboard, has a detector assembly that employs a large area cylindrical array of lead stearate (PbSt) Bragg crystals with a 2d spacing of 100.3 Å. This 2d spacing and the geometry of the detector constrain the instrument sensitivity to the 44-84 Å range.

X-rays enter the detector assembly through an entrance aperture, are Bragg-reflected from the crystal panel, and pass through a collimator and thin window into a proportional counter that is position-sensitive in the dispersed direction. The curvature of the crystal panel assures that at any particular time, different regions of the proportional counter view different regions of the sky at different Bragg angles (i.e., they "see" different wavelengths). When collecting data, the detectors are scanned back and forth so that x-rays from each wavelength interval are collected from a 150° arc on the sky every two minutes. For the January 1993 DXS mission, that arc was along the galactic plane from galactic longitude 150° to 300°. The PbSt may be destroyed by solar ultraviolet radiation and also by atmospheric oxygen atoms hitting it at the Shuttle orbital velocity. To counter

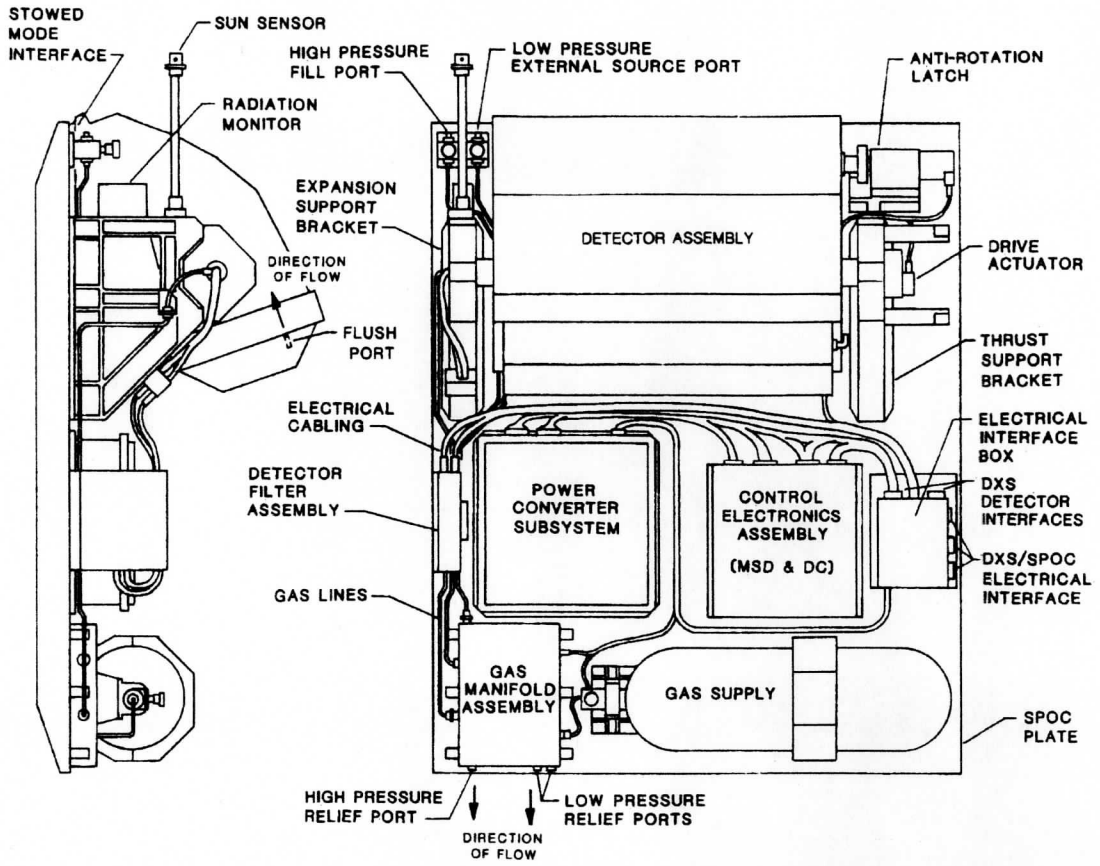

Figure 1. – Layout drawing of one DXS instrument

these effects, DXS is operated only during orbit night and when the Orbiter attitude is such that it blocks the atmospheric oxygen from hitting the crystal panel.

Magnets are mounted at the DXS entrance aperture to reject low energy ($E < 20$ keV) electrons, because the pulses generated in the proportional counter by low energy electrons can mimic low energy x-ray events. The DXS collimator restricts the field of view of any position on the proportional counter to a 15° x 15° (FWHM) sky resolution element. The collimator supports a 100 line-per-inch nickel mesh, which in turn supports the proportional counter thin window against the P-10 counting gas at a pressure of one atmosphere. Each counter has a large-area entrance window made of Formvar and the UV-absorbing agent, UV24, with a total mass thickness of about 90 $\mu g\ cm^{-2}$. The proportional counter has a front layer, where the x-rays of interest are absorbed, and a back-plus-side veto layer that is operated in anticoincidence with the front layer to reject counts that arise from penetrating particles (cosmic rays). Each layer contains anode wires at ≈ 1700 V. Between the two layers is a plane of wires that are at ground potential and oriented perpendicular to the plane of the x-ray trajectory. The distribution of induced electrical charges among these ground plane wires allows the determination of the position of the incident x-ray across the counter, the dispersion direction of the Bragg crystals. The spatial resolution of the proportional counter is about 0.5 mm, but the ~ 2-3 Å energy resolution of the spectrometer is determined by the 15° acceptance angles of the collimator. A more complete description of the DXS instruments is found in Sanders et al. (1992).

3 DXS Science Objectives

At x-ray energies in the band between 0.1 and 0.28 keV, there is a measurable and rather large intensity of diffuse x-rays in all directions. Nearly all of the detected diffuse x-ray flux in this energy band is of Galactic origin and most of it originates closer than ~ 100 pc. In some high latitude, low-neutral-matter directions (e.g., Draco, Ursa Major, Eridanus) there appears to be an additional contribution to the 1/4 keV x-ray diffuse background from the galactic halo. The fraction of the detected flux that is of halo origin is at most 50% in some directions and is negligible over the large solid angle at low galactic latitudes. Halo emission contributes only a small fraction of the total x-ray background seen at this energy. For the past two decades, the low energy x-ray diffuse background has been interpreted as thermal emission from a million-degree plasma in the interstellar medium. This interpretation prevailed because (a) candidate non-thermal mechanisms could be ruled out, (b) the shape of proportional counter pulse-height distributions of the detected x-rays was consistent with theoretical predictions of the emission from a million-degree plasma, and (c) there should be hot plasma in the interstellar medium deposited by supernovae.

The purpose of the DXS experiment is to measure the spectrum of the low energy x-ray diffuse background. The primary scientific objective of the January 1993 flight was to find out if the low energy x-ray diffuse background emission is thermal by seeing if there are emission lines in its spectrum. Astrophysical plasmas in the million degree region are rich in lines, and the relative line strengths carry diagnostic information on the plasma temperature and ionic and elemental abundances.

A second major goal was to identify the wavelengths and strengths of the dominant lines, and from that to determine what elements are the dominant emitters, their states of ionization, and their degrees of depletion or enrichment relative to "standard" abundances. Ionic abundances may be far from the equilibrium values expected for a given electron temperature. The relative ionic abundances provide some promise of deducing the history of the emitting plasma.

A further objective was to determine if the emitting plasma were in thermal equilibrium, its temperature, and something of its history and heating mechanisms.

Another goal of the DXS experiment was to find out if the spectrum of the diffuse background is isotropic, or if there are spectral differences between different directions on the sky that provide additional clues to the evolutionary history of the local hot plasma.

4 DXS On-Orbit Performance

4.1 Summary

The DXS instruments performed well during the entire STS-54 mission. At certain times during the mission, the proportional counters displayed an anomalous behavior that is described in detail in § 4.3. Following the mission, we performed an investigation of this behavior that is described in § 5.2.

4.2 Subsystem Performance

4.2.1 Gas System

Overview. The DXS gas system is designed to supply gas to a proportional counter while on orbit and on the ground. On orbit, the proportional counter pressure is controlled to an absolute pressure of 760 Torr. While on the ground, it is regulated to a gauge pressure of 125 Torr. The system is designed to permit commanded flushing of the counter body gas. A DXS gas system schematic is shown in Figure 2.

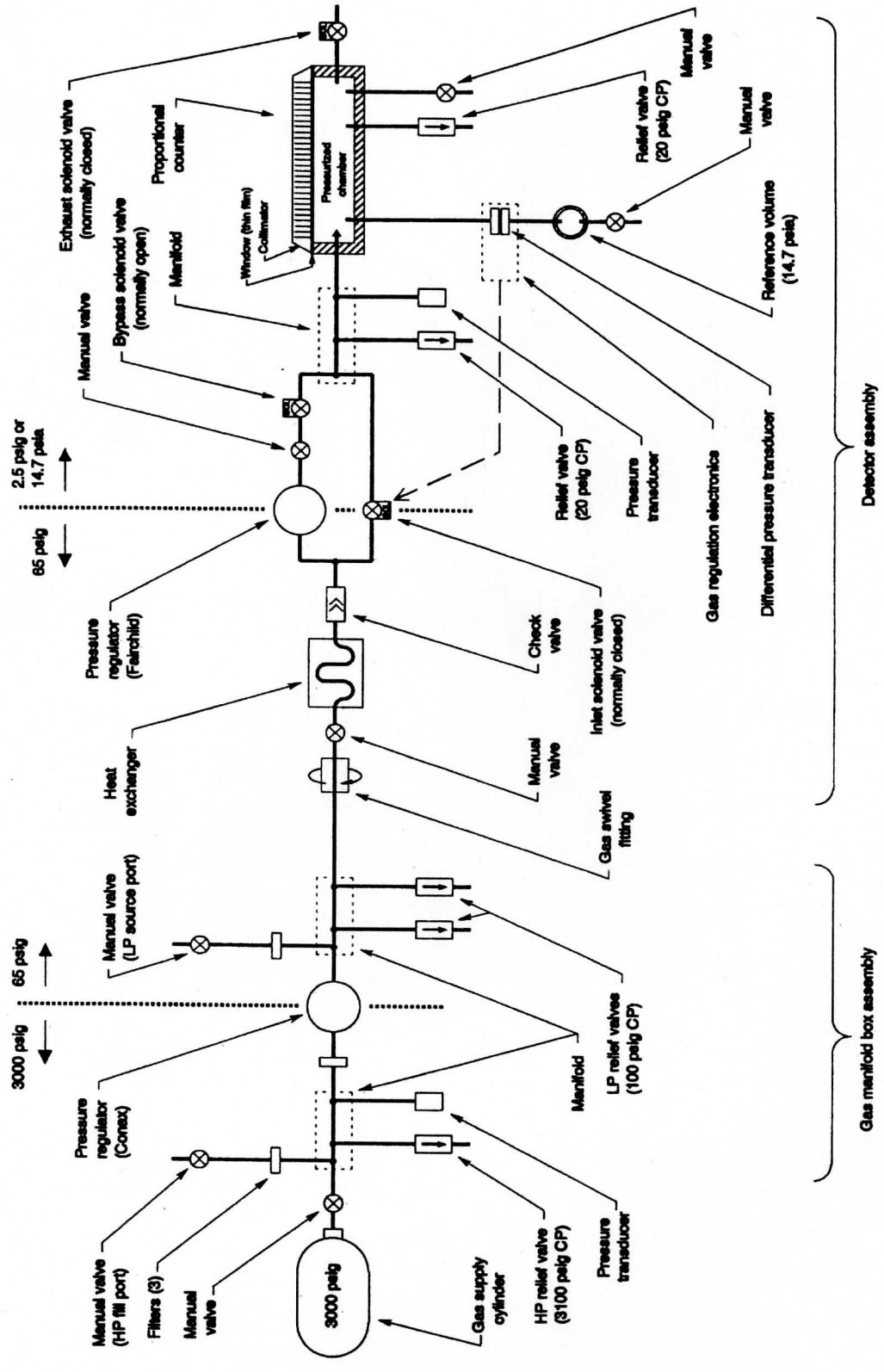

Figure 2 – DXS Gas System Schematic

The DXS proportional counters are rectangular pressure vessels capable of withstanding slightly over one atmosphere of pressure. A magnesium assembly forms five of the six sides. The sixth side is sealed with a thin Formvar/UV-24 window. A typical window is approximately 0.9 μm thick and is supported by a nickel plated mesh. The window material is extremely fragile.

Gas Supply. The on board gas supply has to meet two requirements. It must maintain the pressure in the proportional counter from the final cylinder fill until the completion of the DXS mission operations, and it must permit a once per orbit flush of the entire proportional counter volume. It is also desirable to maintain pressure in the proportional counter until the gas ground support equipment can be connected after landing. The lifetime of the gas supply is directly affected by the leak rate of the Formvar/UV-24 window.

Each instrument has a 0.9375 ft^3 Structural Composites Industries gas cylinder. The cylinder is designed with a fill pressure of 3000 psig which corresponds to a capacity of 192 standard ft^3 (SCF). Due to safety constraints, the cylinders were filled to 2800 psig or 179 SCF. This supply was more than adequate for the Port Instrument. Approximately 102 SCF of gas remained at the completion of the mission. The Starboard supply did last until mission operations were completed, but the supply ran out sometime between the end of mission operations and a week later when the Low Pressure Gas Ground Support Equipment (LPGGSE) was connected.

Ground Gas Regulation. While on the ground, the proportional counter pressure is maintained at 125 Torr above atmospheric pressure using a Fairchild Industrial Products mechanical regulator. The regulator is set to 125 Torr, but has an operational range of 0 - 1520 Torr with supply pressures as high as 500 psig. The regulator is equipped with an internal relief valve. If the downstream pressure rises above the set point, the regulator bleeds off gas until the pressure is at the setting level. Gas may be supplied to the Fairchild regulator from either the gas supply cylinder or through an external supply connected to the instrument. Under normal ground operations, the low pressure gas ground support equipment (LPGGSE) is connected to the low pressure (LP) fill port and supplies gas at 30 psig. The LPGGSE can be equipped to supply either P-10 or nitrogen. For the Fairchild regulator to be operational, the regulator manual valve and the bypass solenoid must be open (see Figure 2).

Mission Gas Regulation. The proportional counter pressure is regulated by the Gas Regulation Electronics (GRE) to an absolute pressure of 760 Torr. The GRE system consists of an electronics box that is connected to the proportional counter gas volume and to a reference volume (see Figure 2). The reference volume is pressurized to 760 Torr absolute at a temperature of 293 °K. The GRE measures the difference in pressure between the reference volume and the proportional counter. When the proportional counter pressure leaks down such that the differential pressure exceeds a preset limit, the gas inlet solenoid is opened and gas is admitted to the proportional counter to raise its pressure.

On Orbit 6, the GRE was powered on and the bypass solenoid was shut. For the most part, the instruments remained on GRE regulation until the instruments were powered off following orbit 90. There were a few orbits in which the instruments were taken to the Hold State and gas regulation was performed by the Fairchild mechanical regulator.

Plots made of the DXS engineering data show the GRE functioning during the mission. Four Port instrument engineering telemetry items are plotted in Figure 3 for orbit 50. The orbit 50 telemetry is typical of the entire mission. The four engineering telemetry items are the difference in pressure between the proportional counter and the reference volume (LDIFFPRES), the inlet solenoid state (LINLETSOL), the exhaust solenoid state (LEXHSOL), and the proportional counter pressure (LCTRPRES).

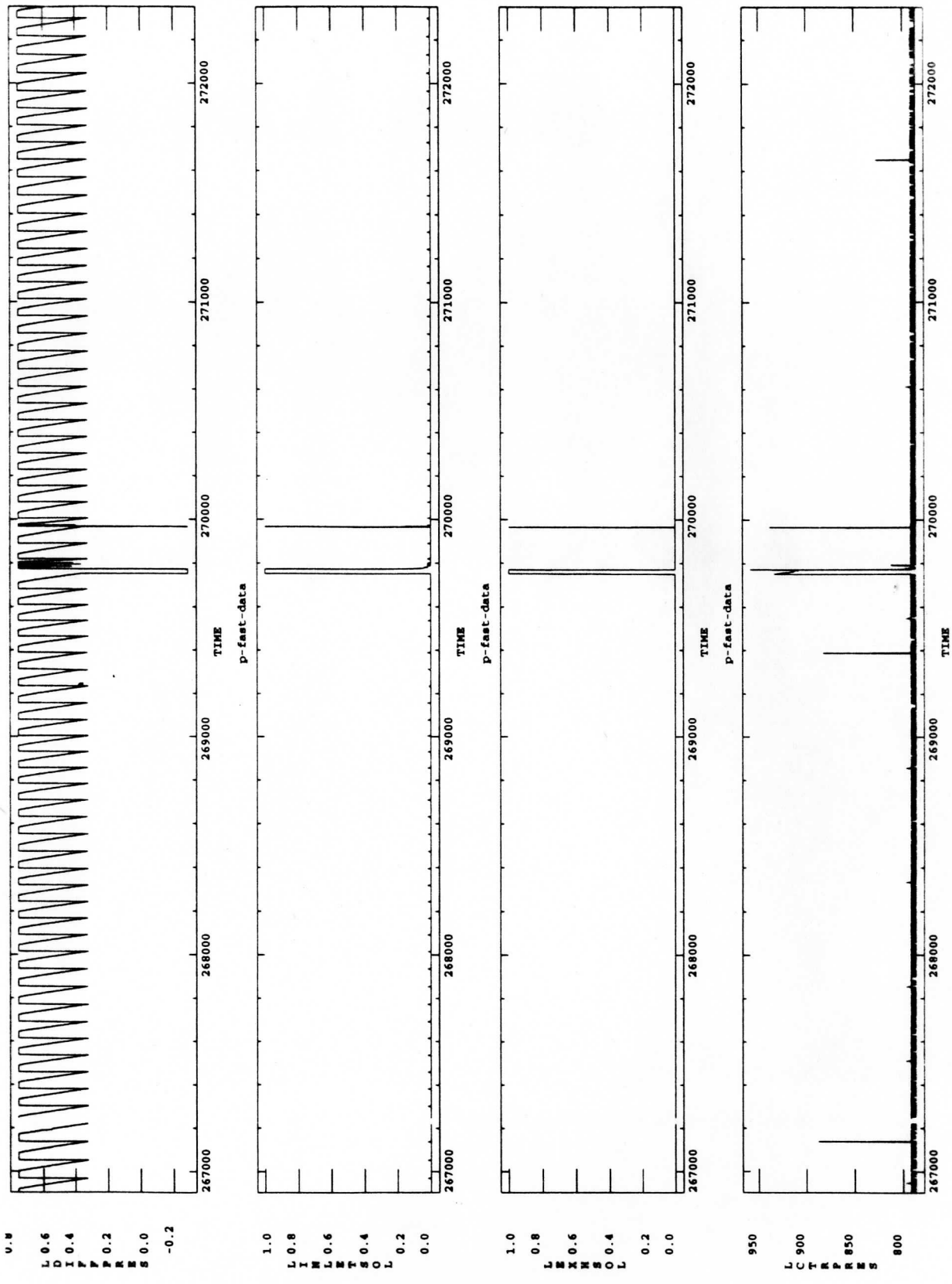

Figure 3. – Orbit 50 data from the Port DXS instrument.

Figure 4 shows a snapshot of the same orbit 50 data seen in Figure 3. The top plot shows the pressure in the proportional counter dropping relative to the reference volume pressure. Once the difference in pressure reaches approximately 0.32 Torr, the inlet solenoid is opened for a fraction of a second to flow gas to the proportional counter. The proportional counter pressure is raised to approximately 1 Torr higher than the reference volume. Therefore, the GRE is capable of maintaining the proportional counter pressure to within ±0.35 Torr.

Flushing the Proportional Counter Gas. The proportional counter gain is a function of three different variables: the proportional counter pressure, the methane / argon ratio, and the high voltage setting. Due to their molecular size difference, the methane diffuses through the window at different rate than the argon. Over time, changes in the methane / argon ratio have an effect on the gain. To maintain the supply gas ratio, the proportional counter is periodically flushed. Flushing is performed simply by opening the Exhaust (or vent) solenoid valve (see Figure 2).

During the mission, flushes were performed about once an orbit. During the later stages of the mission, they were not required on the Starboard instrument as the gas flow through its window was sufficiently large enough to maintain the methane / argon ratios. Figure 5 shows a flush of the Port proportional counter during orbit 50. From the figure it can be seen that the exhaust solenoid was open for 20 seconds. The inlet solenoid opens one second after the exhaust solenoid opens and starts the flow of gas to the proportional counter. The inlet solenoid opens in response to the difference in pressure between the reference volume and proportional volume, and thus does not open until the differential pressure is approximately 0.32 Torr between the two volumes. The inlet solenoid remains open 2 seconds after the exhaust solenoid is closed so the proportional counter pressure is once again 760 Torr. The counter pressure displays a rise in pressure during the flush, but in reality the pressure drops in the proportional counter. Again, this is due to the location of the pressure transducer. The differential pressure curve reveals that the proportional counter pressure is negative relative to the reference volume for the duration of the flush. The flushing system behaved flawlessly throughout the mission.

Gas Heat Exchanger. As gas flows out of the gas supply cylinder it is cooled. The purpose of the gas heat exchanger is to warm the gas to the proportional counter temperature before it enters the proportional counter volume. The gas heat exchanger is located over the proportional counter electronics and transfers the heat from the electronics to the gas (see Figure 2).

During the mission, the proportional counter was most susceptible to a drop in temperature during a flush. Figure 6 shows the temperature plots for the reference volume and the proportional counter body during orbit 50 for the Port instrument. The time frame shown includes the flush plotted in Figure 5. As can be seen in the plot, the neither the reference volume nor the proportional counter body changed temperature during the flush. Throughout the mission, no problems were incurred due to the proportional counter gas being too cold.

Gas System Safety. The gas system was designed to meet or exceed the requirements of NSTS 1700.7B. Specifically, the design is two-fault tolerant from causing the pressure to exceed the Maximum Design Pressure (MDP) of the system. All pressurized lines have an ultimate factor of safety at least equal to 4 and all other gas components at least equal to 2.5. All components and the assembled gas system were proof tested per requirements of NSTS 1700.7B with the exception of two components. The Conax pressure regulator and the high pressure tube assembly were not proof pressurized to 1.5 times their MDP. The test pressure level was only 1.45 times the MDP. This level was accepted by the flight safety board. There were no gas system failures during the mission.

Mission Monitoring. On each orbit, the gas cylinder pressure and inlet solenoid duty cycle were monitored and the gas cylinder pressure was observed. The inlet solenoid duty cycle is an indicator of the window leak rate. Prior to launch, it was known that the Starboard window leaked

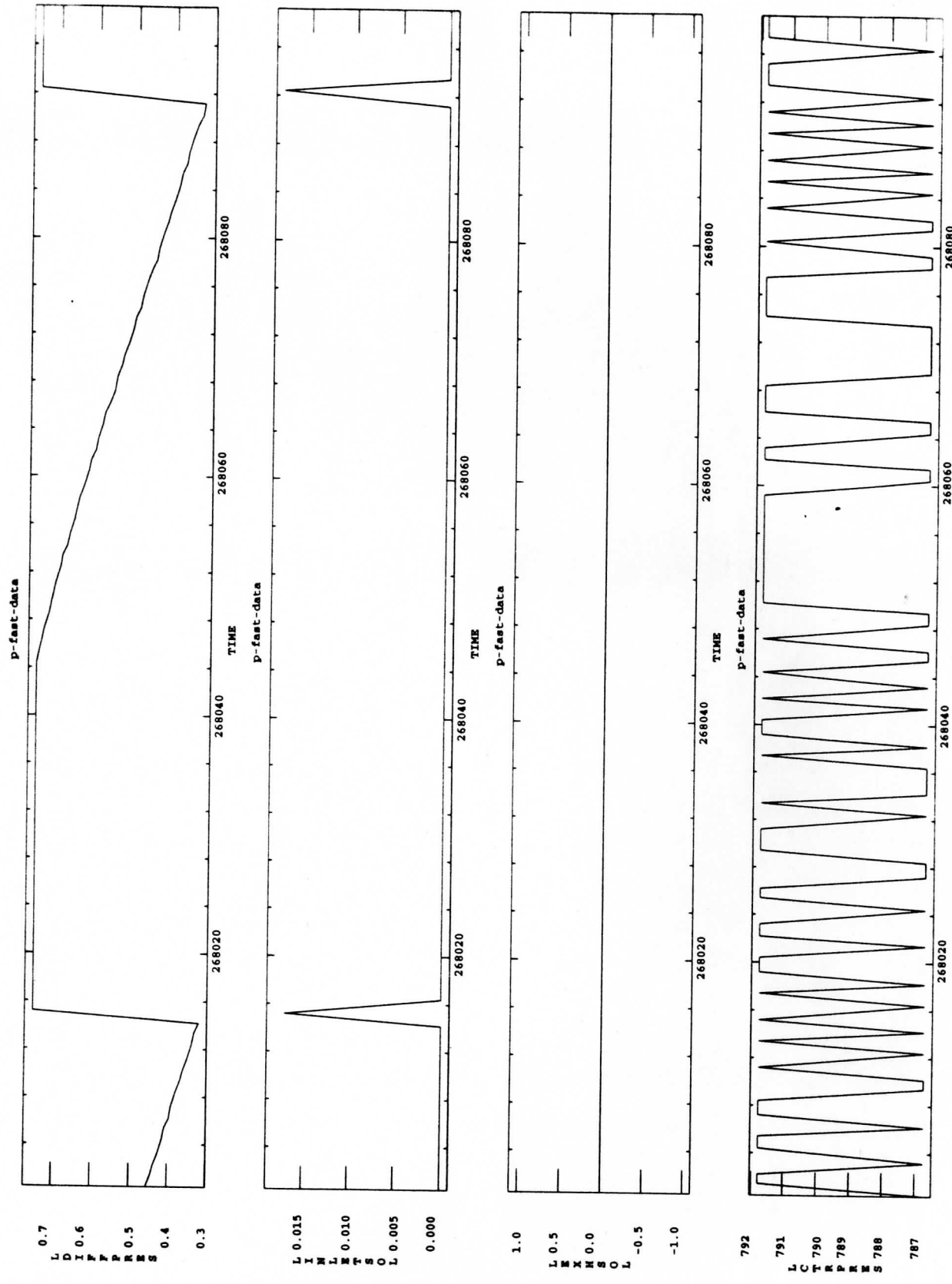

Figure 4. – Orbit 50 data from the Port DXS instrument depicting inlet solenoid firing.

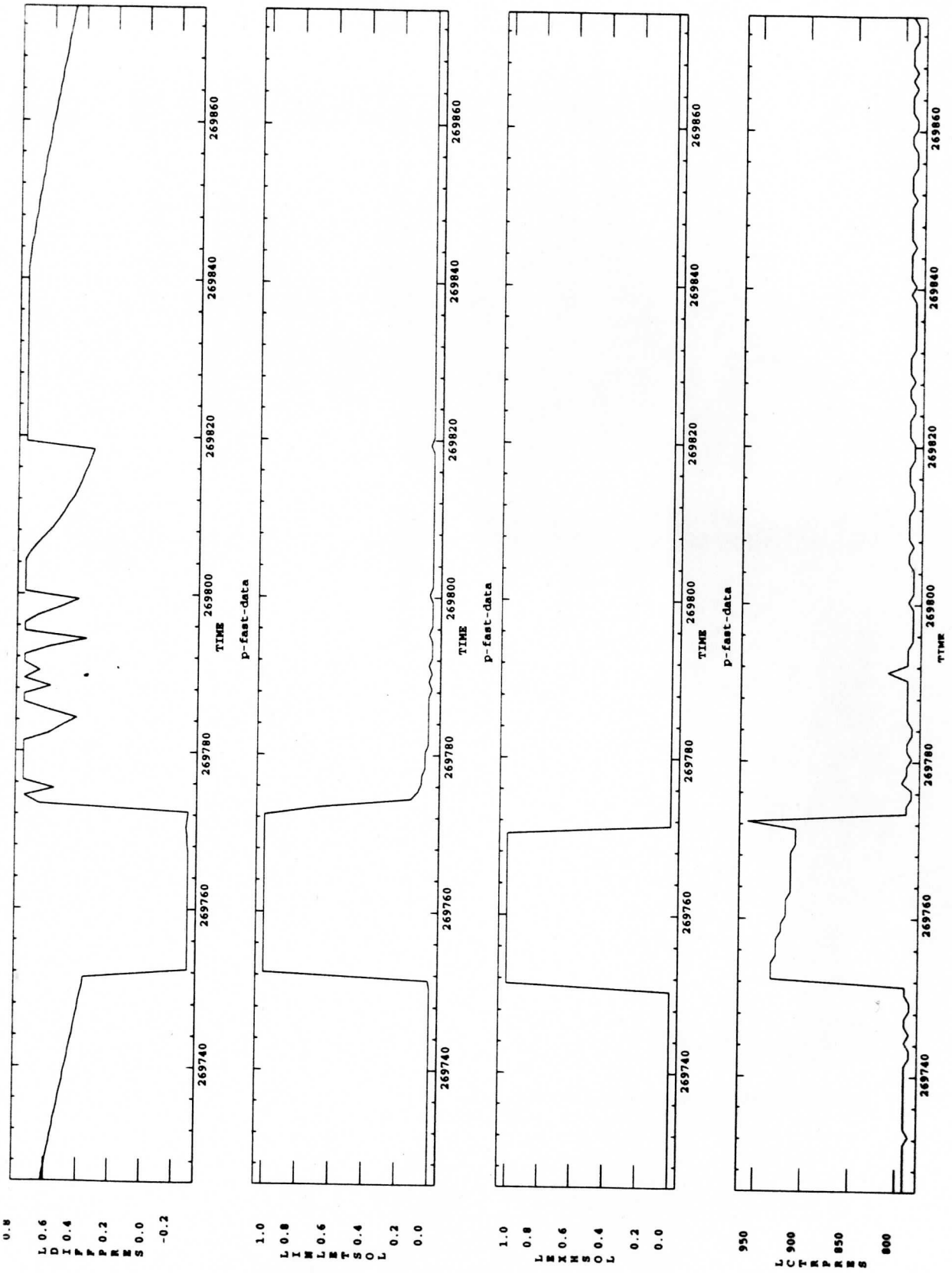

Figure 5. – Orbit 50 data from the Port DXS instrument depicting a gas flush.

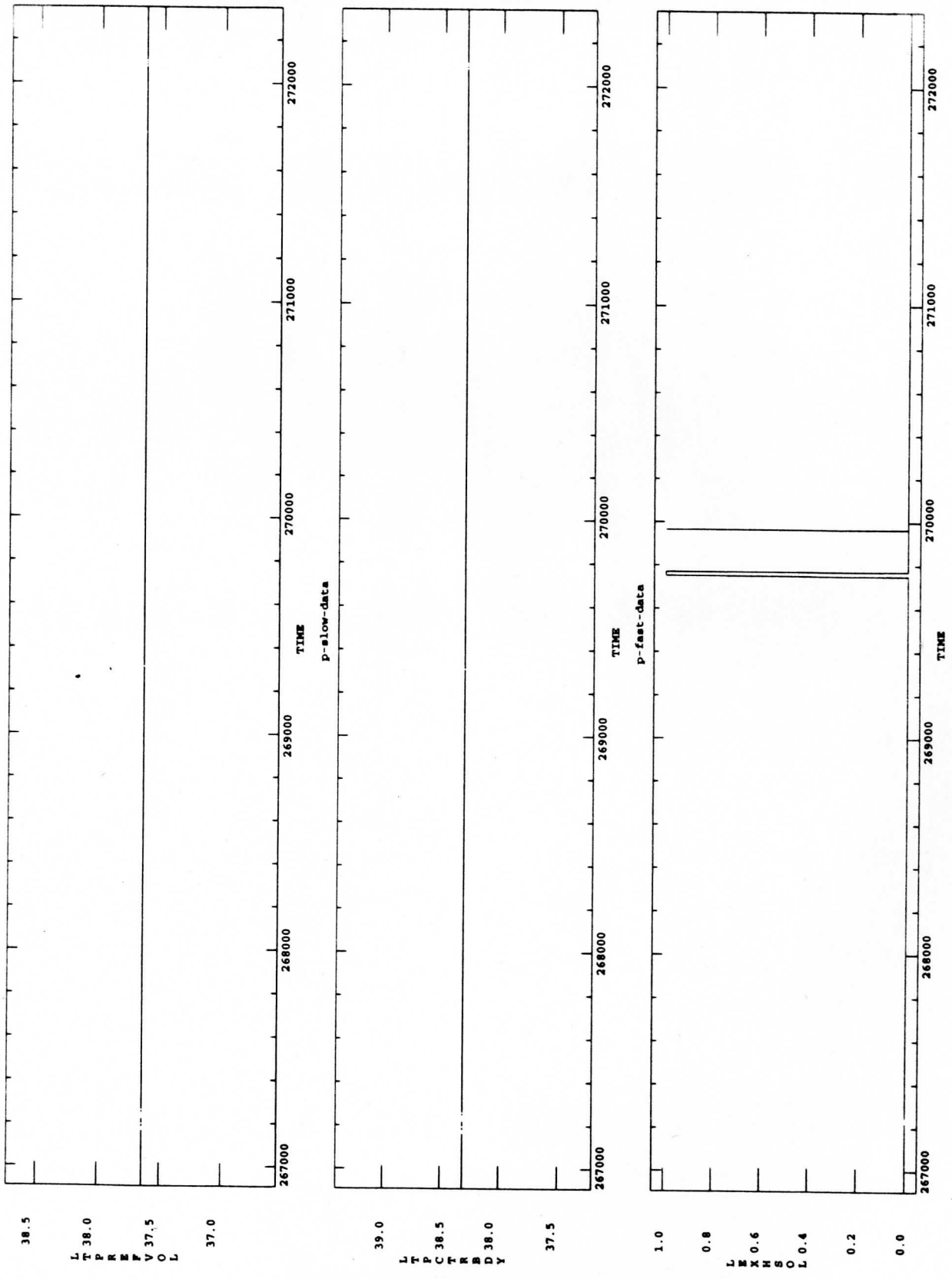

Figure 6. – Orbit 50 data from the Port DXS instrument depicting detector temperatures during a gas flush.

at a greater rate than the Port Window. The last Starboard leak rate measurement prior to launch was done September 30, 1992 and was 7.45 Torr min^{-1} (± 0.10) at 760 Torr. The last Port leak rate measurement prior to launch was on October 8, 1992 and was 0.42 Torr min^{-1} (± 0.04) at 760 Torr. Initially, the Port inlet solenoid was opening (for 0.012 s) once per 180 s, and the Starboard inlet solenoid was opening once per 8 s. The Starboard time between openings was holding between 6 - 8 seconds for the first 20 orbits. Following a couple of instrument state changes between the Standby and Hold states, the rate decreased from once every 4 seconds at orbit 25 to being open approximately 0.012 s s^{-1} for the remainder of the mission. The switching from Standby to the Hold state changed the gas regulation from the GRE to the Fairchild, so the counter pressure is lowered from an absolute pressure of 760 Torr to 125 Torr. This pressure cycling may have had an adverse effect on the Starboard window. It also appears to have had an effect on the Port window. Throughout the first twenty orbits, the inlet solenoid opening interval was roughly 165 - 180 s. Following the state changes, it became once per 75 - 90 s, and remained at that rate for the remainder of the mission.

4.2.2 Drive Assembly and Anti-Rotation Latch

Drive Assembly. The Drive Assembly consists of a drive motor, shaft angle encoder, and speed reduction components that drive the Detector Assembly on a shaft parallel to the orbiter roll axis. During normal data acquisition, the drive rotates the detector back-and-forth through a selectable scan angle, nominally 180° but actually 160° for the DXS mission, at 3° s^{-1}. In response to a stow command or autonomously-generated stow signal, the drive rotates the detector past the normal scan limit to its stowed position. The Drive Assembly interfaces directly to the Motor/Solenoid Driver. A mechanical hard stop limits detector travel to 220° from the stowed position. The drive assembly performed flawlessly during the entire mission. The total scanning time over the course of the mission was approximately 66000 s for each Drive Assembly.

Anti-Rotation Latch. The Anti-rotation Latch secures the detector in the stowed position, preventing rotation about its shaft during launch and landing. The latch mechanism consists of a motor/driveshaft/cam, a detector latch pin, and a variable-stiffness hard stop piston. The detector latch pin, attached to the Detector Assembly, is rotated against the hard-stop piston when the Detector Assembly is in the stowed position. The cam motor is then activated and the cam rotates to compress the detector latch pin into the hard-stop piston. The Anti-rotation Latch uses Hall-effect sensors to indicate latched or unlatched status. No problems were observed with the Anti-rotation Latch during the mission.

4.2.3 Heater System

The heater system on the DXS instruments consists of four independent heater circuits that control the entire detector assembly to a thermal set point of nominally 20° C. The heaters are located on the counter electronics mounting plate, the back side of the crystal panel, and in the aperture throat. Each circuit is autonomously controlled via software with on/off commands issued based on temperature data read from one thermistor per circuit. The Gas Manifold Box is also temperature controlled with its own heater in a similar manner. An additional heater circuit is located on the proportional counter. It is a survival heater which is used only in the event of a proportional counter electronics failure. The temperature set-point for each of the four counter heater circuits and the gas manifold circuit is adjustable by ground command, and the autonomous function may be overridden and disabled by ground command.

During the course of operations the temperature set-point of the four detector assembly heater circuits was adjusted both upward and downward. The heaters were used to elevate the temperature of the detector assembly to as high as +40 °C in order to facilitate the 'bake-out' or warm-up that effectively improved the instrument operations following the early mission anomaly. The heaters, thermistors, and software that comprise the heater system performed without flaw

during the entire mission. Additional independent thermal monitoring via the SPOC Avionics supplied thermistors verified nominal operation of the heater circuits as the temperature set-points were adjusted.

4.2.4 Sun Sensor and Radiation Monitor

The Sun Sensor (SS) and Radiation Monitor (RM) serve as primary detector safing triggers for the DXS instruments. There is one located on each instrument, given that each instrument is in a different environment on the Port and Starboard sides of the Orbiter.

Sun Sensor. The Sun Sensor (SS) consists of five photo-transistors and the associated signal conditioning circuit that converts the summed currents of the transistors to a voltage. At a threshold that is approximately equivalent to the light of the full moon, the SS circuitry indicates to the detector controller (DC) via a digital signal that the DC should stow the detector to prevent UV damage to the crystal panel. Each instrument has its own SS. During the mission the SSs performed flawlessly. Telemetry indicates that the sensors did become active at unique times due to their relative positions in the cargo bay with respect to sun rising over the sills of the Orbiter.

The safing function of the SSs was not exercised during the mission. Orbit observation periods were clearly defined by the Flight Dynamic Facilities (FDF) and command loads to the DXS experiment incorporated sun rise and sunset times according to the FDF products. These command loads ensured that the detectors never started scanning before sunset plus a safety margin, and were stowed by sun-rise, also with margin. There were no unscheduled maneuvers that tripped the sensors.

Radiation Monitor. The Radiation Monitors(RMs), designed to provide an indication of high energy particles and a measure of the density of them, performed nominally during the course of the mission. The RMs were specifically designed to detect high energy particle associated with the South Atlantic Anomaly (SAA), and any other regions that may have been present, and, when a software selectable count rate threshold was exceeded, to signal the detector controller to turn off the detector counter high voltage supplies.

From the post flight data processing we confirm that the RMs count rate during their low activity periods was about ten to fifty counts per minute. During passages through the SAA the radiation monitor count rate typically rose to greater than 10000 counts per minute. At high radiation monitor count rates the radiation monitor DC level becomes triggered and we observed this occurring during the mission and confirm this event in the post flight data analysis. The DC indicator of the radiation monitor typically became active at radiation count rates in the range of 20000 counts per minute. Above this count rate the count rate reported by the RM is unreliable as a result of deadtime considerations for the RM. Other times of high RM count rate activity were during the daytime periods when the RMs were exposed to sunlight (direct or scattered). Solar x-rays sometimes caused significant count rates to be detected during some daytime passages. This count rate did not impact the background data collections that were scheduled for pre- and post- orbit nights.

4.2.5 Proportional Counter

The proportional counter's performances are extensively discussed in §4.1 and §5.2. The prmary cause of the problems that were experienced are thought to be due to flaws or contamination of or on the anode wires. If this experiment were to be re-flown, it would be necessary to install new anode wires and to take greater precautions than in the past to maintain and monitor their health.

4.2.6 Power Control Subsystem

The Power Control Subsystem (PCS) distributes power to the DXS electronics and heaters. DC to DC converters provide the required DC voltages and isolate the DXS electronics from the Shuttle power bus. Relays within the PCS control power to the DXS heaters. All power outputs are fused or current-limited. EMC filters within the PCS minimize conducted and radiated emissions generated by the power converters and switching of heater power. Active inrush current limiters control the turn-on current of the power converters.

PCS performance during both acceptance tests and the flight was within the specifications, and has resulted in no known anomalous instrument performance.

4.2.7 Electromagnetic Compatibility (EMC)

During EMI testing in 1987, the DXS instruments exceeded the radiated emission limits specified in the test criteria (GEVS). The excessive emissions were primarily a consequence of the fact that, because of its design, the proportional counter body had to be electrically isolated from the instrument chassis. Emissions were reduced to acceptable levels by adding filters to the bundle of wires connecting the proportional counter electronics to the Power Control Subsystem and Detector Controller through the rotary coupling. The filters included passive LC common-mode filters as well as differential line drivers and receivers. In addition to the filters on the rotary coupling wire bundle, new Power Cube power supplies and associated power filters were installed in the PCS to replace the original power supplies purchased from Abbott Laboratories.

The instruments were re-tested in 1990 and met the test requirements specified by the test conductor. The levels of emissions were generally well below the GEVS specified levels. Additionally, the instruments displayed no susceptibility to any of the radiated or conducted interference to which they were subjected. In early 1992 the DXS experiment and the SPOC Avionics underwent simultaneous EMI testing as an operating payload component. The DXS experiment exhibited no radiated or conducted emissions in excess of the test levels and demonstrated no susceptibility to radiated and conducted emissions at the specified test levels. During mission operations the DXS experiment exhibited no susceptibility to the Orbiter operating environment, and no problems were reported that indicated any problematic emissions from the instrument. Post-flight data analysis has not revealed any anomalous data problems indicating any type of corruption of the data or artifacts in the data that might be attributable to EMI susceptibility.

4.2.8 Detector Controller Physical Characteristics

The Detector Controller (DC) performs the primary functions of receiving and processing serial command inputs, generating control signal outputs, receiving conditioning and formatting science and engineering telemetry data and receiving and processing data from system sensors. There is one Detector Controller for each instrument, Port and Starboard, with Detector Identification Numbers (ID) embedded in firmware.

Construction and Layout. The physical construction and layout of the DC was driven primarily by the technology available at the time and the architecture selected for this application. Other factors that influenced the implementation are enclosure footprint on the SPOC plate, memory technology, data rate, schedule, inter-board connection technology, and physical layout.

As a result of the considerations mentioned above, the DC circuitry was physically divided between two boards, Upper and Lower, that are contained in the same enclosure. The Upper board contains the ROM for the Science Data Processor (SDP) and the Ku-band Processor (KUP), as well as the three 8088 processors (CPU or Main Processor, SDP and KUP), and other SSI

circuitry the supports the memory block communication between processors; the Upper board is very crowded. The Lower board, at about 50% of chip capacity, has the Random Access Memory (RAM) for the CPU, the system microprocessor clock generation circuitry. the CPU subsection bus interface logic (the CPU is operated in MAX mode, requiring specific bus interconnection logic - the SDP and the KUP are operated in MIN mode), the motor controller processor (MCP - an 8085 processor), and SSI glue logic.

There are a large number of signals that are passed between the two boards through the board interconnection wire harness, as well as a large number of signals that travel from the boards to the DC box level connectors. The internal wire harness for the DC is fabricated from discrete wires soldered to terminals on the boards, or routed to a panel connector (termination in D-style contacts). The wires are formed into a large bundle located at one edge of the board pair, tied tight with lacing cord, and secured to strain relief connections along the edge of the board pair. Wires enter and leave the inter-board bundle as needed to make connections along the board edge or at the front panel connector.

There are two small daughter boards that are mounted above the main boards, one above each board. These daughter boards supply the clock circuit for the serial communications channel and also the random access memory (RAM) interface circuitry required for the shared memory scheme.

Improvements. There was a number of concerns early in the program over the construction of the DC; the concerns focused on the division of the functions of the DC into two separate circuit boards and the inclusion of two daughter boards to complete the functional requirements of the DC. The nature of the construction techniques employed in the building of the two DCs was such that we were virtually guaranteed to have two different units from a hardware standpoint.

Two specific areas of construction that are easily improved upon are in the areas of inter-board wire harness construction, and in circuit division between the boards.

Inter-board wire Harness. Our standard space-flight techniques were used to create the wire harness that communicates signals between the two boards. This technique utilizes discrete wires connected to solder terminals at each board, and the bundles of discrete wires are tied together with lacing cord to form a vibration resistant structure that provides strain relief to the terminations at the solder connections.

This approach is still valid in many applications. In the DCs however, it presented some obstacles. During testing the boards need to be frequently lifted apart, and the bundle served as a constraint on this activity. Additionally, the construction of the inter-board bundle is virtually impossible to reproduce identically from unit to unit.

In future projects that involve designs of this type, i.e. many wires connected to boards that need to be accessed repeatedly, we need to examine alternative approaches. Current technology in wiring and connectors make it very probable that a rugged, flexible, reproducible wiring scheme can be implemented. Some of these options involve mass-terminated coaxial cables, mass-terminated cables with ground planes and shields incorporated, and mass-terminated cables that incorporate special ground plane conductors to provide noise immunity. The mass-termination of the inter-board wire-harness will provide us with the capability to construct multiple units that are very nearly identical in physical construction. Off-board connections, i.e. the signals that leave the DC enclosure for control, telemetry, et cetera, may also be mass-terminated, and will need to be examined on a case-by case basis.

Connector technology has also improved dramatically since DXS was constructed and there are currently available mass termination connectors that will provide all the reliability demanded of a

critical application like the DXS DCs. The benefits accrued in using this technology are lower labor costs and schedule impacts, improved reproducibility, improved reliability, and greater flexibility.

Circuit Function Division. As mentioned above, the circuitry of the DC was divided between two main boards and two daughter boards. This division drove, in many ways, the size and complexity of the inter-board harness. The additional problems of signal skew and timing constraints, cross-talk, and circuit debugging were compounded by the nature of the circuit division.

Technology has advanced sufficiently that such a division would likely be unnecessary now for the same functionality. Additionally, if such a division of circuitry were necessary, we have the awareness of the pitfalls that are present in such and action, and a great deal of care would be taken in the division so as not to complicate issues of testing and reliability. Thorough understanding of the requirements of the specific devices and their timing demands will make it clear what will constitute an acceptable division and what will not.

4.2.9 Detector Controller Performance.

The performance of the detector controllers was excellent throughout the mission. There was a minor surprise in the time keeping subsection of the DC, as explained below. Aside from that singular anomaly both the Port and the Starboard satisfied all requirements and expectations for performance in both the hardware and firmware respects. No unknown operational features reared their heads during the mission, and no "hangs" or other problems with operation occurred.

SDP Resets. During the mission both detectors experienced SDP resets with some regularity. This phenomena was well understood before mission (ref. DXS Memorandum M457, 3/15/91) and was determined not to have a negative impact on the science objectives of the mission. Post mission processing of the time-tagged science events has actually benefited from this reset activity to adjust the time-tags of the science events to compensate for the clock drift of the on-board clock that occurred during the mission (see below).

Time-keeping Overview. The DC keeps time by synchronization of its internal clock with the Avionics provided Pulse Per Minute (PPM). This synchronization occurs when the DXS clock-set command is sent from the ground station to the instrument. Following the setting of the clock, time is kept via interrupts that are driven from divided-down crystal oscillator.

The Time Anomaly. Toward the end of the mission we observed a lack of synchronization between the two detectors scanning cycles. The difference in the time of the turn-around of the scan cycles was about 10 seconds.

Post-mission analysis of the time records that were sent down in the SDP and CPU data streams for the two detectors indicated that the apparent difference in time observed on mission was real. Post-mission data processing has succeeded in assigning the correct time to all events in the data stream. This capability for post-mission time correction is provided by two serendipitous events. One is that both detectors were reset once during the course of the mission. The Port detector was reset at MET 1/01:07, and the Starboard detector was reset as MET 5/05:52. The second serendipitous event is that both instruments had periodic SDP resets as a design feature. This enabled the determination after the fact of how much the science data clock was changing relative to the CPU, and the subsequent attachment of the right time to the time-tagged events in the data stream.

The Cause of the Time Anomaly. The cause of the drift in the DC clocks from the actual time after synchronization is the basis of the time generation in the DC. The crystals that both instrument DCs' clocks are based on have nominal frequency tolerances of (50 ppm. This translates to about

0.18 seconds per hour. A time comparison of the Port instrument time at MET 1/16:32:57, 0/15:25 after it had been reset (at 1/01:07) with the Starboard instrument time at that same 'instant', 1/16:33:01, shows a difference of four seconds, with Starboard fast. Activation was at about 0/01:40. The Starboard instrument had been running for 1/14:53. If the crystal were +50 ppm off in frequency, the Starboard instrument could be expected to be about seven seconds fast. Compared to the Port instrument, it is four seconds fast. At the end of the mission, the Starboard instrument gets reset, and the new Starboard time is about 11 seconds behind what had been present. Both instruments crystals turn out to have about the same variation from the nominal frequency: the Port instrument is about +33 ppm and the Starboard instrument is about +31 ppm.

Future Operations. Future operations with the instruments will entail a periodic setting of the DC clocks by ground command during times that will not interfere with the stored command list execution. This clock set command may be sent as frequently as once per orbit.

Telemetry. Telemetry downlinks during mission exhibited no anomalous behavior and performed as expected for both the Port and the Starboard instruments.

Command. Command uplinks and DCs reception, processing and execution of command during mission operation was nominal, with no exceptions to expected behavior.

Scan Motor and Latch Motor Control. Scan motor operation by the MCP in the DCs was nominal during mission operations. There were no observed problems during the mission, and angular pointing of the detectors as indicated in the post-mission processed data is smooth and glitch-free. The latch motor was operated by command during the mission and the control circuitry for that mechanism performed flawlessly.

Thermal. Thermal modeling of the DC prior mission and thermal-vacuum test verification of the models proved to be a reliable indicator of performance during mission operations. No anomalous temperature excursions were manifested by the DCs during the mission and thermal performance of the DCs was nominal.

4.2.10 Electron Rejection Magnets

There are permanent magnets inside the Detector Assembly used to deflect low energy electrons entering the detector. They appear to have worked very well during the mission. The strongest field is at its source and is 200 Gauss. Figure 7 shows the DXS magnetic field for one instrument.

4.3 In-Flight Anomaly

4.3.1 The Starboard Instrument Malfunction Prior to and at Orbit 10:

The performance of the STBD (Starboard) detector as judged by the engineering data alone appeared to be normal prior to orbit 10 at MET (Mission Elapsed Time) 52810. The STBD lower veto rate (LCLVETO) had been well below the lower veto threshold (L-Veto, LCVETOTHR) rate of 4000 s^{-1} and the high voltage was switched on and off by the radiation monitor crossing its effective threshold (LRMTHR).

The filtered event rate data (main anode pulse heights, PH, in the range 140-800, goodness of fit, GOF, in the range 1-20 and position, POS, in the range 20-220) tell a different story. During the scanning time for orbit 7 the event rate was about 1 s^{-1} while before and after the scanning period the event rate was small, about 0.2 s^{-1}. The event rate just after the orbit 8 scanning period increased markedly from its previous 0.2 s^{-1} to 1 s^{-1}, and then experienced another increase of the post-scan event rate to > 10 s^{-1} in orbit 9. The event rate during the pre-scanning period of orbit 10 continued to increase, following an increase of the radiation background as measured by the

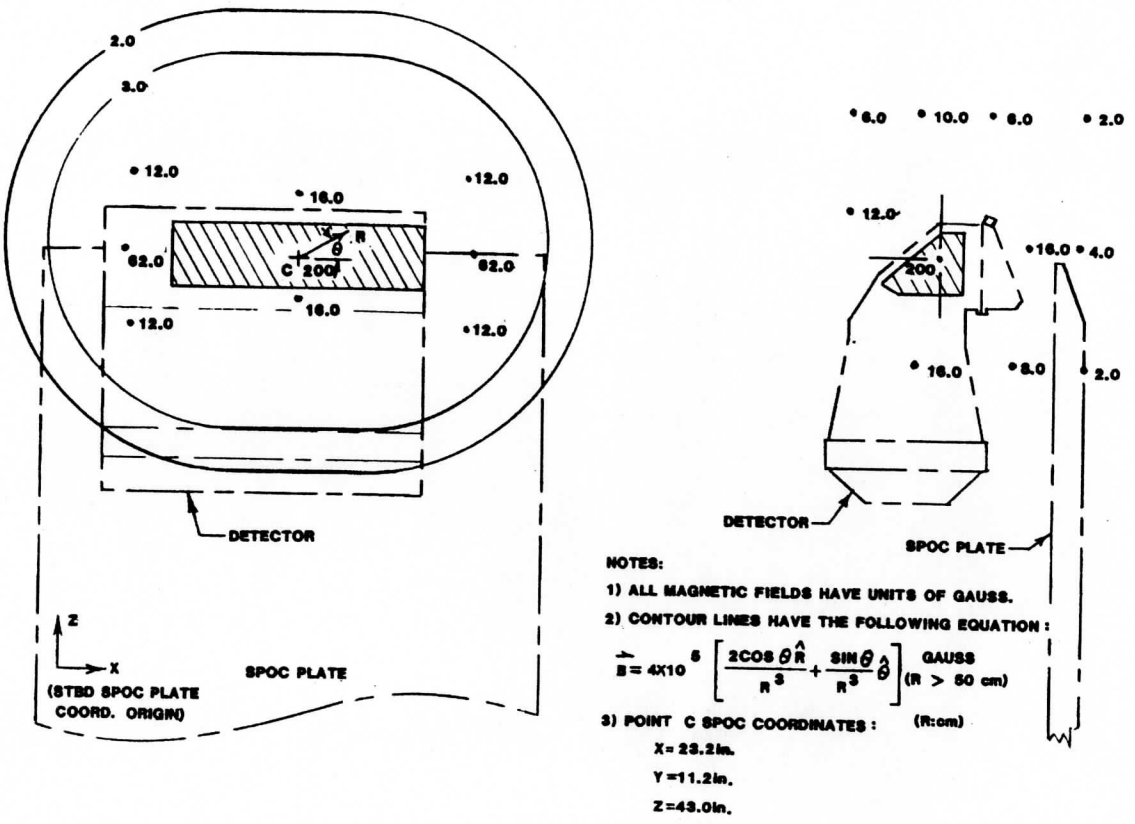

Figure 7 – DXS Magnetic Field

radiation monitor. Examination of the POS-PH plots reveals that most of the events are from 3 or 4 broadly defined positions ("hot bands or hot smears") and suggest anodes with contaminated areas. The apparent sudden drop in the event rate at MET 51980 s was due to a science data processor (SDP) reset. The five-fold increase of the filtered event rate starting at MET 52500 s appears related to increases in the scaler count rates described below.

Just before MET 52810 s both the PORT and STBD veto and main anode raw count rates (CLVETO and CLMAIN) had increased by a factor of two to five, having started the increase at MET 52600 s. The PORT rates decreased after the peak at MET 52810 s and returned to normal by MET 53200 s. It seems clear that the counter radiation background varied as indicated by these PORT rates. The geographic location of the shuttle at this time suggests strongly that this radiation was associated with the South Atlantic Anomaly (SAA). Both radiation monitors had percentage variations at this time that were similar to but smaller than the veto and main anode raw count rate variations. Both RMs exhibited broad increases centered at MET 52000 s but this feature is not present in the veto or anode rate records. Both instruments were in their stowed configuration at MET 52000 s so the radiation that was responsible for the RM rate increase was unable to penetrate the proportional counter shielding materials. Shortly after MET 53000 s the PORT instrument started scanning. There were no discernible changes in the veto or main anode count rates of the PORT detector at this time.

The STBD CLVETO rate mirror that of the PORT data until MET 52810 s when there was a sharp spike in the LCLVETO count rate to greater than the 4000 s^{-1} threshold. This spike caused the Detector Controller to turn off the STDB detector high voltage and there was established a temporary RMVETO value of about 28. There followed several (automated) attempts to turn the high voltage back on. Following the initial attempt there were five more, spaced 30 seconds apart,

since the associated LRMVETO values, taken at 30 second intervals, happened to be successively smaller. There followed four more attempts at times determined by when the radiation monitor happened to have a measured rate smaller than the LRMCOUNT value recorded when the high voltage was last turned off.

At about MET 53750 s the STBD LVETOTHR was changed by uplink command from 4000 s^{-1} to 8000 s^{-1}. Consequently, the high voltage, following its turn-on at MET 53810 s, stayed ON because the LCLVETO rate stayed below 8000 s^{-1}. Nevertheless, the LCLVETO values in the 200 s interval between MET 53810 s and MET 54010 s were far in excess of those of the PORT counter at this time. In addition the STBD deadtime monitor (DT) was pegged at 96% and there were jagged features suggestive of high voltage breakdown on the LCUVETO record. The event rate during this 200 s interval was high and characterized by poor GOF parameters indicative of events or sparks or leakage originating at positions other than along the anode wires. The 200 s interval was terminated at MET 54010 when the high voltage was turned off by ground command.

4.3.2 The Port Instrument Malfunction at Orbit 11:

The PORT instrument performed correctly and well during orbits 7,8,9 and 10. The filtered event rate was typically small when the instrument was stowed and increased to about 1 s^{-1} during scans. At MET 57730 s the high voltage was turned off to accommodate a gas flush procedure and at MET 58180 s the high voltage was turned on and the PORT calibration X-ray tube activated for a routine and successful gain calibration. From MET 58170 s until MET 58467 s the deadtime and the LCLVETO, LCUVETO, LCLMN and LCUMN rates were normal, as was the filtered event rate. Both PORT and STBD LRMCOUNT rates were low and normal. AT MET 58467 s the PORT DT jumped to 96% while the PORT main anode and veto rates (except LCUMN) were irregular and jumped about by large factors. The telemetered rate for the LCLVETO dropped in accord with its known overload property. The filtered event rate was very small, probably as a consequence of large DT. At MET 58500 s, 33 seconds after the high veto rates appeared, the PORT scanning motion started. Hence the high rates cannot be attributed to the sudden exposure of the instrument to the space rather than a shielded environment. Further, the output of both RMs remained nominal and (statistically) constant during this whole period. The jagged and high veto and anode rates with abrupt changes are uncharacteristic of radiation-induced records, and it appears that the behavior of the PORT (and the STBD) instrument was due to some on-board phenomena such as high voltage breakdown within the gas volume or in the high voltage circuitry.

4.3.3 The Starboard Instrument, Orbits 11-90:

During orbits 11-18 there were attempts made to turn on the STBD and PORT high voltages. These attempts were unsuccessful, apparently because the continuing counter malfunction produced excessive LCLVETO rates. During the scanning period of orbit 19 the STBD high voltage could be left on and was, but the DT was pegged at 96% and continued to be pegged during orbits 20-23 during high voltage-on periods. The veto and main anode raw count rates of the STBD instrument during orbits 20-23 were uncharacteristically noisy and the high voltage was turned off. The high voltage was not turned on successfully, despite numerous attempts, until orbits 32 and 33. During these two orbits the DT, main anode and veto raw count rates all looked normal, but the filtered event rates were 5 s^{-1} or more, indicative of hot spots. The high voltage was not turned on again until orbit 39 and performance through orbit 44 improved, but the filtered event rate was still excessive. The high voltage was then turned off as part of a warmup and was not turned on again until orbits 48-50. The pattern that evolved for the remainder of the available DXS orbit time was to collect data until the counters became noisy or suffered breakdown. There followed a period of slightly elevated counter temperature with the high voltage turned off. This seemed to clean up the counter malfunction for a few to several orbits. It is not understood why this clean-up procedure was even partially successful.

4.3.4 The Port Instrument, Orbits 12-90:

During orbits 12-20 several attempts were made to turn on the PORT high voltage. During orbit 20 the PORT high voltage could be turned on and was left on. But the veto and anode records were high and irregular indicating near-continuous high voltage breakdown. The DT was 96% and the overall picture was very much like the experience of orbit 11. During orbits 21-26 there were several unsuccessful attempts to turn on the high voltage. Finally, during orbit 27, the high voltage was turned on successfully and the DT, veto and anode records were all normal although the filtered event rate was very large. Good performance with satisfactory filtered event rates was evident during orbit 28 and continued through most of the remaining orbits with brief warmups during orbits 62-64 (because of a scheduled EVA) and orbits 84-86. During orbit 59 the high voltage was off due to either high veto rates from background or breakdown malfunction. The data from orbit 76 are confused and there may have been telemetry drop outs. As with the STBD instrument, the warmups were effective but the reason for their success is not understood.

4.3.5 Analysis

The filtered event rate from the STBD detector increased during orbits 8,9 and 10 and this increase appears to be a result of hot spot formation on the anode wires. The ambient radiation background, as determined by the RMs and by the various counting records of both the STBD and PORT detectors, cannot have been the cause of this filtered event rate increase. The ambient radiation background did increase, reached a maximum at MET 52800 s, and at this instant some sort of serious counter malfunction began.

While the STBD malfunction occurred during a time in which there was clear evidence of high ambient radiation intensity, the PORT malfunction originated during a radiation-quiet period. There was no indication of extraordinary radiation from either of the RMs or from the DT, main anode or veto raw count rates of the PORT instrument itself. The malfunction started while the instrument was stowed and it was not until 33 s later that detector scanning and the resultant exposure of the thin window counter to the sky occurred. Hence the first malfunction of the PORT instrument occurred in a benign radiation environment. Whatever the cause of this anomalous event, the LCLVETO circuitry did not turn off the high voltage promptly and the breakdown was allowed to continue for more than 400 s. The cause of the eventual high voltage turn-off at MET 58940 s is uncertain. The apparent spike in the LCLVETO record does not appear to exceed the then-current value of 4000 s for LVETOTHR.

In summary we seem to have encountered two basically different types of counter malfunction.

1. Hot spots or hot smears
   These are characterized as telemetered events that satisfy the standard filtering criteria and are only distinguished from normal x-ray events by the fact that an unreasonable number cluster about or occur at the same x-position. It is difficult to see how these can arise from other than from damaged or dirty areas of the main anode wires.

2. Leakage pulses
   These are events that characteristically have no or meaningless position information. The ground plane pulse heights are all essentially zero and the main anode or event pulse height distributions are of the approximate form 1/PH. Lack of ground plane pulses shows that the electron or ion motion that was the origin of the anode charge pulse occurred outside of the proportional counter gas volume. Likely places are leakage in the anode wire end seals, leakage in the signal by-pass capacitors or leakage in the high voltage wiring in the potted end cavities. These sorts of malfunction would be expected to show up in a vacuum environment. These malfunctions were <u>not</u> evident during the thermal vacuum tests.

5 Post-Flight Activities

5.1 Post-Flight Calibrations

The DXS post-flight calibration began following the completion of the anomaly investigation on the flight instruments. The main goals of the calibration were to (1) develop a response matrix with a calibrated wavelength scale to fit the calibration data, (2) measure the Effective Area-Solid Angle ($A_{eff}\Omega(E)$) product of the detectors as a function of photon energy and (3) measure the flatfield response of the proportional counters.

Initially, three line sources were calibrated for intensity and uniformity. The line sources consisted of aluminum panels with a sheet or coating of carbon, boron, or zirconium. Mounted on either side of the panel were ^{210}Po sources. The sources were angled towards the panel to illuminate the carbon, boron, or zirconium target to produce Kα x-rays from the carbon (277 eV) and boron (188 eV) targets and Mγ x-rays from the zirconium (151 eV) target.

The first two goals were met by placing each detector assembly in a large vacuum chamber and exposing it to each line source. The line sources calibrated the wavelength scale from 151 - 277 eV and produced three energy distributions to compare to the developed response matrix. The line sources permitted a comparison of three independent $A_{eff}\Omega(E)$ calculations.

The proportional counter flatfield response measurement was done separately. The goal was to measure what pattern of events versus position would be produced when a counter is uniformly illuminated. This distribution or proportional counter response can then be divided into the flight data to remove any proportional counter non-uniformity effects from the data. To accomplish this, the proportional counter assembly was placed in a vacuum chamber and the carbon line source was positioned over the collimator. Each of the 14 anode wires was exposed individually to insure a uniform illumination and to look at each individual wire for non-uniform responses.

To complete the calibration, the flight windows and meshes were mapped. Mapping measures the transmission of the window and mesh in discrete positions. Each window and mesh were mapped in a 4 x 8 grid using the carbon, boron, and zirconium energy lines. The mapping checks for any non-uniformities in the window and produces a "map" of the window contours. The measured transmissions are then folded into the flight data analysis.

5.2 In-Flight Anomaly Investigation

5.2.1 Statement of the Problem

During early mission operations of the DXS mission, while performing observations during orbits seven, eight, and nine, the proportional counters in the Starboard and Port instruments developed a behavior that we have characterized as "elevated count rates". Specifically, we observed an elevated count of detected events in the proportional counters, up to the maximum event rate of the data system, and an increase in the deadtime of the counters to about 95%. Ultimately the instruments' safing mechanisms turned the counter high voltages off. The instruments were not behaving as predicted, and the consensus at the time was that the counters' performance deterioration had been initiated by a very large flux of ionizing radiation encountered while the high voltage was on. The Port and Starboard instruments behavior was independent of each other; the Port instrument seemed less affected.

Instrument performance was recovered by the "baking out" of the counters at an elevated temperature, e.g. 40° C, for up to several orbits. The difference in instruments allowed us to utilize the Port instrument more than the Starboard; the Port instrument required less frequent bake-outs and typically recovered nominal operation sooner than the Starboard. However, the problem was

recurrent. During subsequent operations the instrument performance degraded with time, even though we operated very conservatively, shutting the high voltage off by command during SAA passages, and closely monitored event rates and deadtimes. In each case of performance degradation, the instrument science team made a judgment call as to when performance was unacceptable, and instrument nominal performance was recovered by baking out over several orbits.

The degradation of performance of the proportional counters during the flight exposure is characterized by the following phenomena, obtained from post-flight data analysis:

- The appearance of faulty position information, suggesting the presence of anode "hot spots".
- High veto and main anode raw counting rates during periods when the ambient radiation was believed to be normal.
- High rates from one anode set accompanied by very low rates from another set suggesting a continuous discharge that loads down the high voltage.
- A decrease in gas gain that did not recover as expected following gas flushes.

Typical veto and main anode count rates under normal conditions in flight were 500 s^{-1}. For a five day flight, assuming no high voltage off periods, and no periods of much higher rates, we have a total of (500x3600x24x5)=2 x 10^8 counts.

5.2.2 Tests

Most of the tests we have performed have been directed to understanding the effect of a large flux of ionizing radiation on the operation of the counters. To minimize impact on the DXS instruments all tests save one were performed on a small single wire counter. One test with the Starboard flight instrument involved exposing it to ^{60}Co for an extended period of time using a gas supply that was of the same type used for flight. The test counter body was about a foot long, 1.5" x 1.5" in cross-section and had a single anode wire of the same type wire used in the DXS flight counters. There were no position-sensing ground potential wires and the counter body formed the cathode. The inside surface of the counter was coated with Aquadag colloidal carbon. The window was of aluminized Mylar supported by a nickel mesh and a strongback with square holes. The filling gas was P-10 of the same type that was used in flight.

To simulate the on-orbit high-flux events, two sources were used: ^{60}Co and ^{55}Fe. The ^{60}Co 1.2 MeV gamma rays result in secondary electrons more or less uniformly distributed through the counter volume and so simulate roughly the in-flight environment. The ^{55}Fe radiation consists of nearly monoenergetic X-rays of 5.9 keV and was collimated to produce a fan beam that had a width of 1.2 mm (0.047 inches) at the counter wire position.

Following the laboratory exposures, the test counter performance was evaluated as described below. These three points were designed to reveal malfunctions of the type expected.

- Response to ^{55}Fe x-rays at a standard place on the anode was measured as an indication of the gas gain.
- The ^{55}Fe source was moved along the length of the counter to search for possible hot spots or high or low gain.
- The background level as measured by a threshold discriminator set to 90 eV, just above the amplifier noise, was measured.

5.2.3 Single Wire Counter Test Results

After initially small but subsequently large exposures to ^{60}Co radiation, and after a total exposure of 1.1 x 10^9 counts, none of the malfunctions suggested by the on-orbit phenomena were generated by the tests a, b, or c above.

Similarly, after varying exposures of ^{55}Fe radiation, and after a total exposure of 3.1×10^9 counts, none of the malfunctions suggested by the on-orbit phenomena were generated. All of these counts were registered by one particular 1.2 mm segment of the anode wire. This was a particularly stringent test if one expects the number of counts per unit length of the anode wire is the important factor in causing malfunction. Our test count density was then $(3.1 \times 10^9$ counts) / (1.2mm) = 2.6×10^9 counts mm^{-1}. The count density for the nominal 2×10^8 counts experienced in orbit would be only 3.1×10^4 counts mm^{-1} since there were 14 wires, each 12 inches long, and the 2×10^8 counts were presumably equally distributed along the total length of the anode wires.

There was some evidence for continuous discharge of the counters in flight. We drove the test counter into a discharge condition by raising the supplied voltage and measuring the discharge current. During the most severe test the anode wire carried 2260 volts and drew 0.24 microamperes for 10,000 seconds. The gas flow was reduced to zero for this test. The counter voltage was then returned to its nominal value (1750 volts), the counter gas flush restarted so as to replace all the gas and the usual tests mentioned above were carried out. The only sign of malfunction was a reduction of the gas gain by about 20% indicated by the pulse height distribution using ^{55}Fe. The total charge transferred during the 10,000 seconds was 2.4×10^{-3} coulombs. The charge transfer implied by the on-orbit 2×10^8 counts was 5.7×10^{-5} coulombs. During an earlier similar test of 10,000 seconds with the gas flow still operative, the gas gain showed no decrease.

Following the above tests, a test on the quality of the gas used in flight was performed. Speculation that there might be microscopic particles in the gas that would cause momentary hot spots was explored. These particles would be at the "bottom" of the on-board bottle until orbit is achieved, at which time they would become suspended in the gas in the micro-gravity environment of orbit. To explore this hypothesis a bottle of P-10 gas used to fill the on-board bottles was inverted and remained in that configuration for several days, to allow any particles in the bottle to settle at the regulator end of the bottle. Following this period of time, the single wire counter was then exercised in the manner described above for the exposure tests, with gas supplied from the inverted bottle with particles, if any, mixed with the gas. This test demonstrated that there was probably no contaminant in the gas that would have caused the phenomena that we observed on-orbit.

5.2.4 ^{60}Co Tests on Starboard Counter

To determine if anode hot spots could be induced on the flight instruments using ^{60}Co, the Starboard counter was exposed to a ^{60}Co source mounted above the collimator. After several hours, the anode wire under the ^{60}Co source did develop a hot spot which caused the instrument automatic safing function to turn the high voltage to the counter off. Several attempts to turn the high voltage on again following removal of the ^{60}Co source resulted in automatic turn-off virtually instantaneously. Following an overnight "non-operation", about 16 hours, the Starboard instrument was again operated and the high voltage was turned on. There was at this later time no evidence of the hot spot that had been induced by the ^{60}Co exposure.

The results of this test imply that time is a factor in the curtailing of hot spot activity. The temperatures that we used on orbit are not particularly "hot", but may have accelerated the removal of hot spots that would normally occur over a longer time interval at room temperature.

5.2.5 Conclusions

We have been unable to repeat the phenomena that was observed on orbit on the single wire counter, and we have not been able to repeat the on-orbit gain depression and faulty position information on the flight instruments using localized exposures of the counters to ^{55}Fe and ^{60}Co. We have been successful at introducing a hot spot on the Starboard counter using ^{60}Co, which disappeared following an overnight rest.

It may well be that the counter configuration of the single-wire counter is sufficiently different from the flight instruments that we will be unable to replicate the on-orbit phenomena. For instance, during calibration tests at Space Physics we observed that a small counter with a Formvar window would charge up and the gain would subsequently be decreased. The aluminized Mylar window on the single wire counter used for the test described above would prevent that charging from occurring, and consequently we would not see a gain depression. The flight instrument windows are Formvar, and we have not seen the instruments exhibit a depressed gain during vacuum chamber tests.

The geometry of the single wire counter is significantly different from the flight instruments. This may affect our ability to replicate the on-orbit phenomena.

Further analysis of the flight data may yield insight into what the causal factors involved in on-orbit instrument operation. This analysis may lead to conclusions that suggest further, significantly different tests, to be performed either on single wire counters, or on the flight instruments themselves.

5.3 Data Reduction

The reduction process to convert the dxs raw data to the reduced format consists of four steps. The first step takes the data in the raw files and separates them into the associated fits files. These fits files contain independent information: fast engineering data, slow engineering data, science data, ancillary orbit data, ancillary SPOC data, and time data. Each of these files is then filtered to remove duplicate events. The second step consists of determining the position of the instrument at each time. From this are computed the solar azimuth, solar zenith, terrestrial latitude, terrestrial longitude, galactic latitude, and galactic longitude for each event record. At this time, the wavelength of the recorded photons for each channel is written into the data files. The third step consists of filling in any missing data points. These missing points are the result of position blackouts in the satellite orbits. These dropout points are corrected by interpolating the position on either side of the dropout along a great circle connnecting the points before and after the dropout. The last step consists of applying a gain correction to the science data. Since the gain in the counter changes over time, the recorded pulse heights have to be corrected for the change in gain over time to normalize the data. Finally the binned spectra are corrected for the effects of a non-uniform proportional counter response as a function of position across the counter - the "flat-field" correction.

5.4 Data Analysis

5.4.1 The Hot Interstellar Medium and the Soft X-ray Background

The DXS observations are observations of the low energy ($0.1 < E < 0.28$ keV) X-ray background. This low energy X-ray background has been interpreted for the past 20 years as thermal emission from a hot (million degree) phase of the interstellar medium, even though direct evidence was lacking that the emission was thermal or that it originated in the interstellar medium (ISM). In the past few years, ROSAT observations have strengthened the case that the origin of the soft x-ray background is the ISM, and the DXS observations discussed here indicate that the emission is indeed thermal, although even the relevant temperature is still uncertain.

The appearance of the soft X-ray background can be seen in the all-sky maps produced by several experiments (McCammon et al. 1983, Marshall and Clark 1984, Garmire et al. 1992, Snowden 1993, Snowden et al. 1995) in the C band or the 1/4 keV band. The post-ROSAT general picture is the following. The finite intensity of the soft X-ray background seen in the plane of the Galaxy requires that there be a "local" component, closer than the closest 10^{20} cm^{-2} of neutral material.

The local ISM is known to be relatively empty out to 50 - 100 pc, so this local cavity is a natural place for the local X-ray background component to originate. In at least one direction (MBM 12, G154-34) the local component is known to originate closer than 65 pc from the Earth (Snowden, McCammon, and Verter 1993). Some directions, generally at high galactic latitudes, are brighter than other directions, generally at low galactic latitudes, because the local emission component extends farther *out* of the galactic plane than it does *in* the galactic plane, and because there is a galactic halo emission component that provides up to 50% of the total in some high latitude directions. There are other interstellar cavities (e. g., Orion/Eridanus, Monocerous/Gemini, Scorpius/Centaurus) that also contain soft X-ray emitting regions that are seen from Earth. Sanders (1995) presents schematic diagrams of some major features of the local interstellar medium relevant to the emission of the soft X-ray background.

5.4.2 Previous Spectral Observations of the Hot ISM

Before the flight of DXS, the only spectral information about the diffuse background was obtained from the distribution of pulse heights recorded by proportional counter detectors. The observations with the best spectral resolution were those of Inoue et al. (1979), who used a gas scintillation proportional counter. These pulse height distributions were typically found to be consistent with the X-ray spectrum predicted to be emitted by a plasma in collisional ionization equilibrium with normal cosmic abundances at a temperature near 10^6 K, plus or minus about 30%, independent of the particular plasma model that was used. In addition to the detailed pulse height distributions, the ratios of counting rates from one pulse height band to another also were consistent with million degree plasma. Since no viable non-thermal mechanisms could be identified, and since supernovae were perfectly acceptable thermal mechanisms, the "standard" interpretation became that the source of the low energy X-ray diffuse background was a 10^6 K collisional plasma in the interstellar medium.

5.4.3 Results from the Diffuse X-ray Spectrometer

DXS obtained spectra of the diffuse background with 2 - 3 Å spectral resolution over the 83 - 44 Å range. The field of view was mechanically collimated to 15°, and it scanned an arc along the galactic plane that covered the longitude range 150° - 300°. Thus, it obtained spectra from the local hot bubble component of the diffuse x-ray background, but not from the halo component.

The DXS scan path covered well-known features of the diffuse x-ray sky, such as the Monoceros/Gemini enhancement, which is possibly a fossil supernova remnant, and the Vela supernova remnant, as well as more "typical" unenhanced regions along the galactic plane in Auriga, Puppis, and Crux. Figure 8 shows the spectrum DXS obtained from the Puppis region, longitudes 213° - 252°. The solid line shows the data, with one sigma error bars, while the dotted line shows the best fit single temperature Raymond & Smith model. The best-fit temperature is 1.16 x 10^6 K, with an emission measure of $n_e^2 d = 0.0026$ cm^{-6} pc. These are reasonable values, roughly the same as those found by previous experiments (McCammon and Sanders 1990), but in detail the fit is not acceptable. Most noticeable is the 61 Å - 75 Å region, where the data exceed the model substantially. Also quite apparent are the region near 76 Å, where the Mg VIII line of the model does not stand out in the data, and the 54 - 55 Å region, where the Si IX and S IX lines of the model are not prominent in the data.

In Figure 9, the solid line shows the spectrum that the Port DXS instrument obtained from the Puppis region, longitude 213° - 252°, with 1 σ error bars, while the dotted line shows the best fit single temperature Mewe & Kaastra model. The best-fit temperature is 1.14 x 10^6 K, with an emission measure of $n_e^2 d = 0.0034$ cm^{-6} pc. These are again reasonable values, but the fit again is not acceptable. Most noticeable is that in the 63 – 79 Å regime the data exceed the model, but it is not as discrepant in the 64 - 68 Å regime as the RS model is. Also apparent are the region near 61 – 62 Å, where the Si VIII line of the model strongly exceeds the data, and the region near

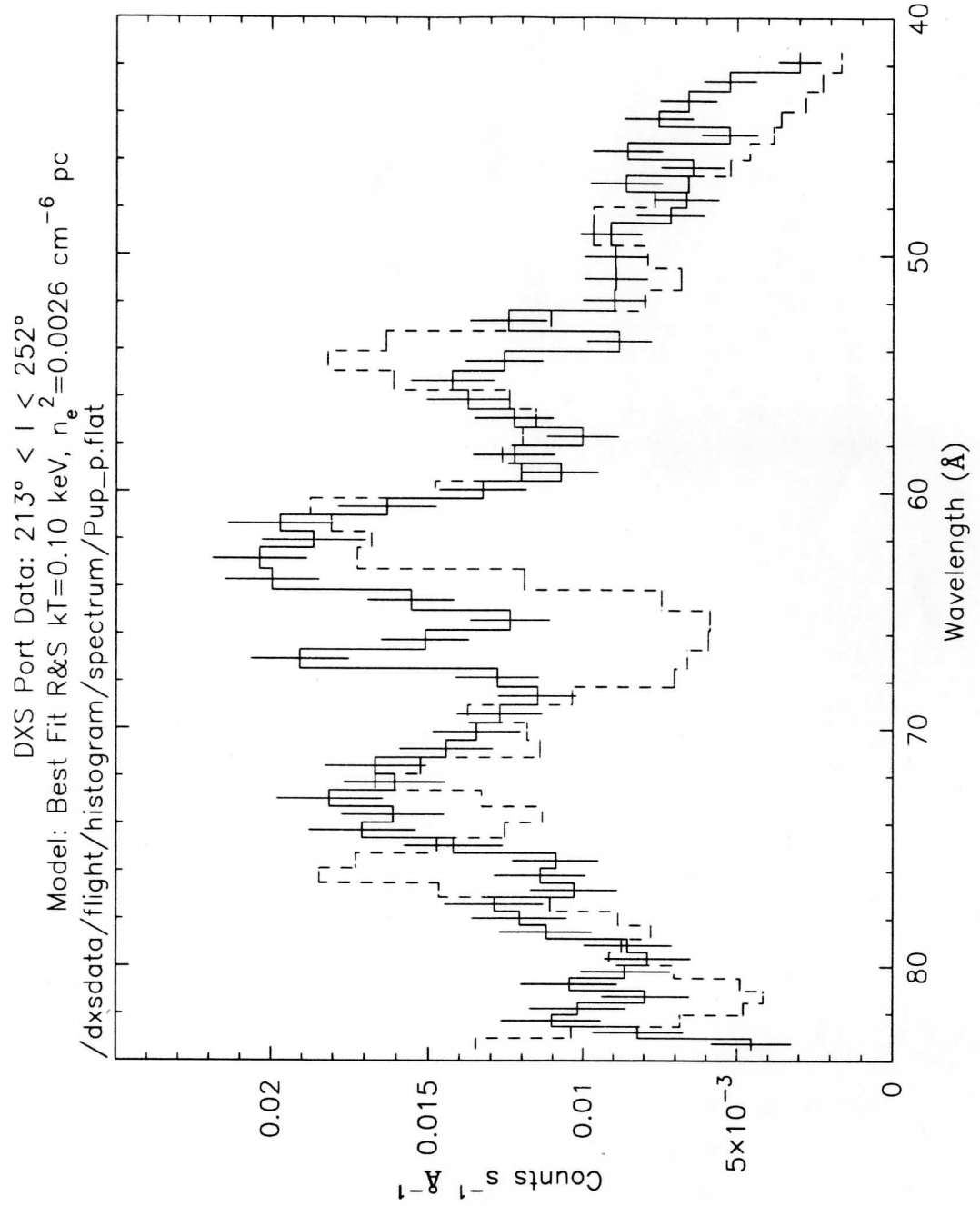

Figure 8 – DXS spectrum from Puppis (solid line) and best-fit single temperature coronal plasma model from Raymond & Smith (dashed line).

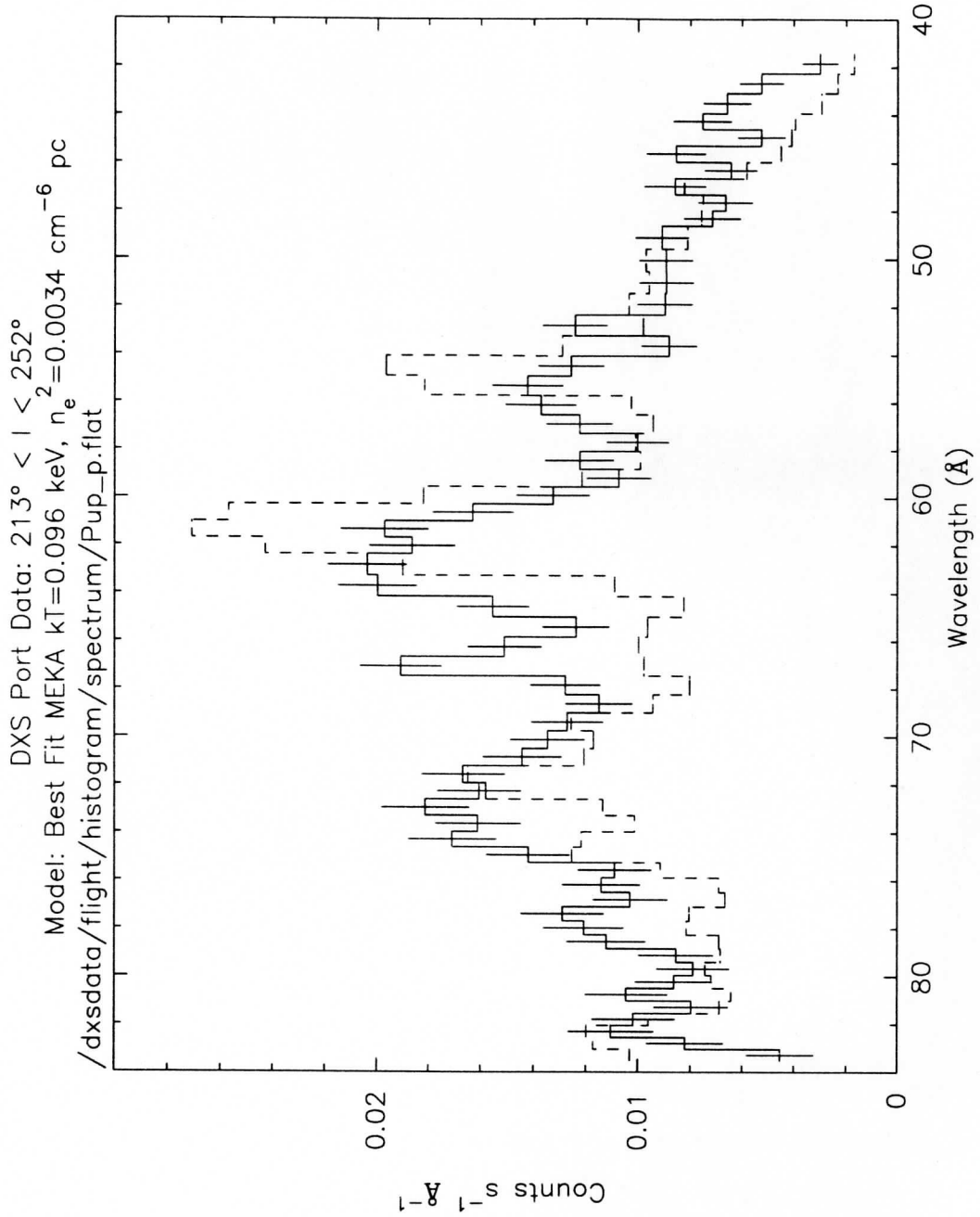

Figure 9 – Best-fit single-temperature Mewe & Kaastra model (dashed line) compared to the DXS data (solid line)

55 Å, where the Si IX line of the model strongly exceeds the data. Note that this is the same Si IX line that Raymond & Smith have at 54.5 Å (see previous subsection) and that Liedahl has at 55.5 Å (see below).

Two-temperature fits were examined, and looked promising with one temperature near one million degrees and the other near 2.5 x 10^6 K, but the required emission measure of the higher temperature component over-produced X-rays in the 0.5 - 1 keV range by a factor of 5. Various NEI models were also examined, blast wave and cooling plasmas, as well as depleted abundance plasmas, but all without success. Abandoning fits with the standard models, we next tried the approach of fitting the spectra of individual ions, with the goal of setting upper limits on the column density of individual ions. In doing this however, we discovered that there are significant differences between the synthetic spectra generated by the Raymond & Smith code versus those generated by the Mewe & Kaastra code. As the differences between the synthetic spectra generated by the RS code and those generated by the Mewe & Kaastra code became apparent, it was unclear which code to use. D. A. Liedahl of Lawrence Livermore National Laboratories, using the HULLAC atomic physics package, recently calculated improved atomic data for selected ions of Si and S and Mg, and from these obtained the emission spectra of those ions at a temperature, kT=100 eV, appropriate for the DXS data analysis. Spectra of selected ions of iron at kT=200 eV were also calculated.

In Figure 10, the dashed line shows the spectrum of Si at kT=100 eV (T=1.16 x 10^6 K) calculated from the RS code, folded through the DXS response function, and plotted with an arbitrary normalization. The solid line shows the spectrum of Si at kT=100 eV, obtained from the individual ion spectra calculated by HULLAC and the ionization balance calculated by the RS code, folded through the DXS response function and plotted with an arbitrary normalization. The shapes of these two spectra are significantly different - enough so that we think future work must incorporate the HULLAC results.

Currently 18 ionic spectra (Mg VII -- X; Si VII -- XII; S VII -- X; Fe XIII -- XVI) have been calculated at one temperature each (kT=200 eV for Fe; kT=100 eV for the others) using HULLAC. We anticipate that the spectra of the above ions, and possibly a few others, at a number of temperatures in the range of interest will be calculated soon. In the meantime, we have tried fitting the DXS Puppis and also the Monoceros-Gemini data using the only the 18 single temperature ionic spectra that we have. The reduced chi-squares are still too large to consider these acceptable fits, but large improvements over the plasma code models are already apparent. We think that we will be able to make significant progress in fitting the DXS spectra after the results of additional calculations using HULLAC become available.

5.4.4 Summary

1. The low energy X-ray background shows evidence for lines, implying that we are observing a hot phase of the interstellar medium.
2. The detected spectra do not match the model spectra of cosmic abundance equilibrium plasma for $10^5 < T < 10^6$ K.
3. We have not yet found a collisional ionization equilibrium model with depleted abundances or a model of a non-equilibrium plasma that fits the data. We may need improved models.
4. The data show evidence for different spectra in different directions.
5. We need additional data, particularly at high latitudes, as well as in other low latitude directions. Better signal-to-noise would help, also.

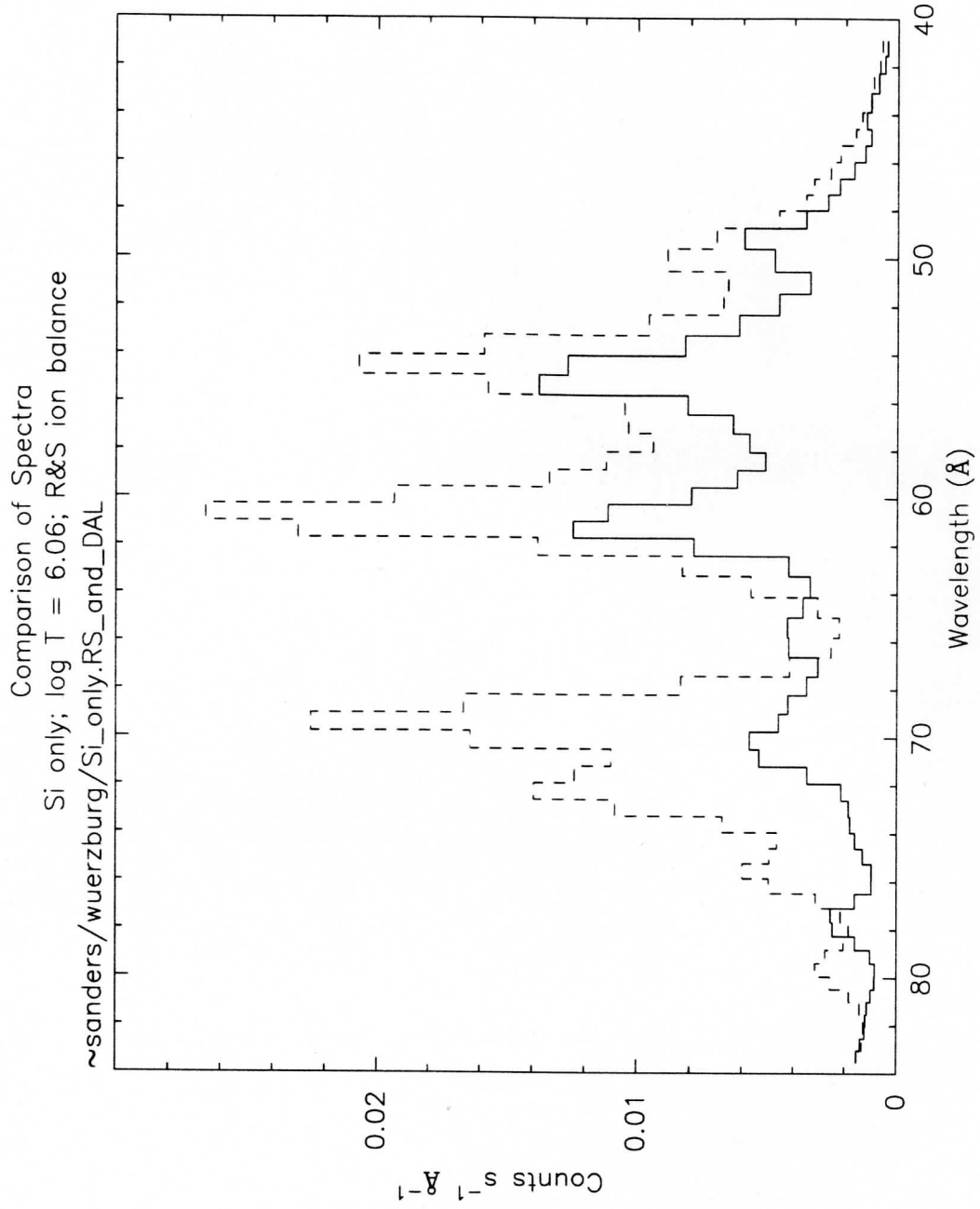

Figure 10 – Si spectrum at log T = 6.06 calculated using RS model (dashed line) and a Si spectrum at log T = 6.06 calculated using HULLAC (solid line)(arbitrary normalization).

6 References

Garmire, G. P., Apparao, K. M. V., Burrows, D. N., Fink, R. L., & Kraft, R. P., 1992, ApJ, 399, 694

Inoue, H., Koyama, K., Matsuoka, M., Ohashi, T., Tanaka, Y., & Tsunemi, H. 1979, ApJ, 227, L85

Marshall, F. J., and Clark, G. W., 1984, ApJ, 287, 633

McCammon, D., Burrows, D. N., Sanders, W. T., & Kraushaar, W. L., 1983, ApJ, 269, 107

McCammon, D., & Sanders, W. T. 1990, Ann. Rev. Astr. Ap, 28, 657

Sanders, W. T., Edgar, R. J., Juda, M, Kraushaar, W. L., McCammon, D., Snowden, S. L., Zhang, J. & Skinner, M. A. 1992, in *EUV, X-Ray, and Gamma-Ray Instrumentation for Astronomy III*, Oswald H. W. Siegmund, Editor, Proc. SPIE 1743, 60

Sanders, W. T., 1995, in *Physics of the ISM and IGM*, eds.A. Ferrara, C. F. McKee, C. Heiles, & P. R. Shapiro, ASP Conf. Series, 80, p. 498

Snowden, S. L., 1993, Adv. Space Res., 13, (12)103

Snowden, S. L., Freyberg, M. J., Plucinsky, P. P., Schmitt, J. H. M. M., Trümper, J., Voges, W., Edgar, R. J., McCammon, D., & Sanders, W. T., 1995, ApJ, 454, 643

Snowden, S. L., McCammon, D., and Verter, F., 1993, ApJ, 409, L21

7 Appendix

High Dose Laboratory Tests.

A likely cause of the hot spot or hot smear phenomena was thought to be a high dose of radiation and in particular a large number of detected particles per unit length along the anode wire. To investigate this possibility we did a number of tests using a small laboratory counter. The counter body was about a foot long, 1.5 x 1.5 inches in cross section and had a single coaxial anode of the same type wire as used on the DXS counters. There were no position-sensing ground potential wires and the counter body formed the cathode. The window was of aluminized Mylar supported by a mesh and strong back with square holes. The filling gas was P-10 of the same type used in flight.

Two types of radioactive sources were used in these tests, ^{60}Co and ^{55}Fe. The ^{60}Co 1.2 MeV gamma rays result in secondary electrons distributed more or less uniformly throughout the counter volume and so simulate roughly the in-flight environment. The ^{55}Fe radiation consists of nearly monoenergetic x-rays of 6000 eV and was collimated to produce a fan beam that had a width of 1.2 mm (0.047 in) at the counter wire.

During most of the tests a flow rate of 0.147 cm^3 sec^{-1} of P-10 was maintained in a successful attempt to keep constant the counter gas pressure and gas gain. The gain was checked frequently by taking pulse-height distributions of the ^{55}Fe source. The gas gain was about 8000 and the high voltage was kept at 1750 volts. For reference this gas flow corresponds to about 24 times the leak rate per unit volume of the Port counter and 1/3 the leak rate of the Starboard counter.

A detected ^{55}Fe x-ray with a gas gain of 8000 results in a charge pulse on the anode of 2.8×10^{-13} Coulombs. The amount of charge produced from ^{60}Co progeny is widely distributed but on the average is within a factor of 2 or 3 of that for ^{55}Fe. The initial serious malfunctions of the counters followed 3 or 4 orbits of operation during which the veto and main counting rates were typically 500 sec^{-1} for the combined area of 20 sec^{-1} for each of the 24 main anodes. Later in the flight following the "warm rest cure" routines there were periods of 10 or so orbits of good performance. We estimate that if doses of high radiation intensity were responsible for the observed malfunctions of the DXS proportional counters the critical number of counts per anode before malfunction is in the region of 10^6. If density of detected counts along the anode is the more significant quantity, the critical density is about 4000 counts mm^{-1}.

Following the exposures described below, the performance of the test counter was evaluated and examined for malfunctions. The pulse height distribution was taken with the ^{55}Fe source at a standard position. This was meant to reveal shifts in gas gain. The collimated ^{55}Fe source was moved along the counter face with the fan beam normal to the anode. Pule height distributions were examined in a search for hot spots. Also, with the sources removed the counter background level was measured and tracked. For this test the discriminator threshold was set to 90 eV.

After initially small but subsequently large exposures to ^{60}Co no malfunctions were evident. The total number of counts at the end of this test was 10^9 or a thousand times as large as the supposed threshold.

Similarly, after initially small but subsequently large exposures to the fan beam ^{55}Fe source no malfunctions were evident. The total number of counts recorded in this test was 3×10^9 in a 1.2 mm length of anode wire. This represents a dose about 10^6 times the hypothetical threshold.

As mentioned earlier there was some evidence for continuous discharge of the counters during flight. In order to examine and evaluate this phenomena we drove the test counter into a discharge condition by increasing the high voltage to 2260 volts where the anode continuous average current was 0.24 μamps. This current was maintained for 10^4 s and represented a charge transfer of 4.4×10^3 Coulombs. The gas flow was reduced to zero during this test and the only malfunction noted was a 20% loss in gain. An earlier similar test with the gas flow maintained so as to keep the gas pressure constant resulted in no measurable gain change.

In summary, we have been unable, using the test counter, to reproduce malfunctions of the type observed in orbit.